Chemical control of friction: mixed lubricant monolayers

O.K. Dudko[a,*], A.E. Filippov[b], J. Klafter[a] and M. Urbakh[a]

[a] *School of Chemistry, Tel Aviv University, 69978 Tel Aviv, Israel*
[b] *Donetsk Institute for Physics and Engineering of NASU, 83144 Donetsk, Ukraine*

Received 26 December 2001; accepted 22 February 2002

Controlling frictional behavior in nanoscale sheared systems can be made possible when the relationship between the macroscopic frictional response and the microscopic properties of the sheared systems is established. Here, a new approach is proposed for tuning the frictional response and obtaining desirable frictional properties. This tuning is achieved through shear-induced phase transitions in a mixed lubricant monolayer consisting of a base solvent and an additive. The interaction between the solvent and additive molecules and their relative concentrations are shown to be the major parameters in determining the magnitude of the friction force and the nature of the response (stick–slip or sliding).

KEY WORDS: friction; control; embedded monolayers; phase transitions; additives

1. Introduction

Recently introduced experimental tools that allow detailed investigations of friction at nanometer scales have led to a major increase in activity in the study of interfacial friction on the microscopic level [1–8]. Dealing with frictional properties over the nanometer scale, nanotribology offers a meeting ground for practical aspects of friction with new and fascinating physical phenomena such as dynamic phase transitions, giant enhancement of viscosity under confinement, shear-induced chaos, memory effects and more [9–14].

The field of nanotribology revolves around the attempt to understand the relationship between macroscopic frictional response and microscopic properties of sheared systems. What one wishes to deduce from experimental observations and from theoretical modeling are new insights that will help establish the origins of friction forces, differentiate among different embedded systems (lubricants), maintain the desired types of motion and control frictional forces.

Controlling frictional forces has been traditionally approached by chemical means, usually supplementing base lubricants by friction modifier additives [15,16]. Each additive in such molecular mixtures has a different role: some decrease static friction and eliminate undesirable stick–slip motion, some influence the temperature dependence of viscosity, others inhibit corrosion [15,16]. While the behavior of single-component lubricants in nanoscale confinements has been extensively studied both experimentally and theoretically [1–14], investigations of the behavior of molecular mixtures under similar conditions are in their early stages [17,18]. Questions on frictional forces of mixtures, regimes of motion, stability, microscopic behaviors of the additives and their interactions with the base lubricants and substrates are still open.

In this paper we propose a new approach that helps in deciding on how to tailor molecular mixtures so that they provide desirable frictional properties. Tuning friction is achieved here through shear-induced phase transitions in the mixed embedded system. We focus on the relationship between the macroscopic frictional response and microscopic properties of the sheared molecular systems such as intermolecular interactions and relative concentrations. Understanding the molecular picture would then allow one to create desirable phases of motion and to control frictional forces.

2. The model

In order to mimic surface forces apparatus (SFA) experiments on sheared confined liquids [1–4] we introduce a model that consists of two rigid plates, with a monolayer of N particles each of mass m at locations $\mathbf{r}_i = \{x_i, y_i\}$ embedded between them (figure 1). One of the plates of mass M and center-of-mass coordinate $\mathbf{R} = \{X, Y\}$ is pulled with a linear spring of spring constant K. The spring is connected to a stage that moves with velocity $\mathbf{V}$. This system is described by $2N + 2$ equations of motion:

$$M\partial^2\mathbf{R}/\partial t^2 + \sum_i^N \eta\partial(\mathbf{R} - \mathbf{r}_i)/\partial t + \sum_{i=1}^L \partial U^{\mathrm{A}}(\mathbf{r}_i - \mathbf{R})/\partial\mathbf{R} + \sum_{i=L}^N \partial U^{\mathrm{B}}(\mathbf{r}_i - \mathbf{R})/\partial\mathbf{R} + K(\mathbf{R} - \mathbf{V}t) = 0 \quad (1)$$

*To whom correspondence should be addressed.

1023-8883/02/0500-0217/0

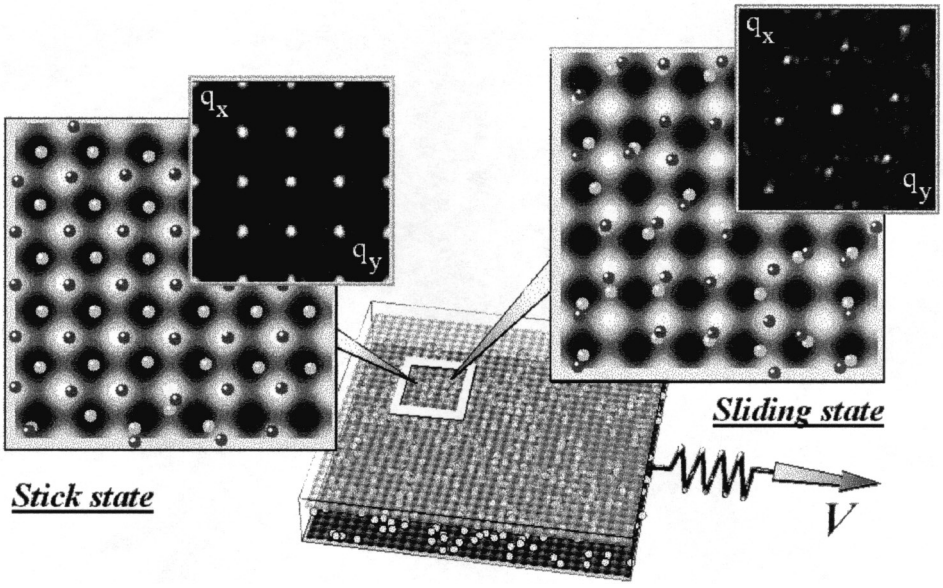

Figure 1. Schematic representation of the model geometry and snapshots of the sheared monolayer showing a tetragonal lattice for the locked states and a hexagonal one for the sliding states. The insets show the corresponding correlation functions. Parameter values: $N = 200$, $M/m = 0.7N$, $\eta = M\omega/N$, $q = 0.9(U_0 a)^{1/2}$, $K = 80U_0/a^2$, $c = a$, $C = 2U_0$, $k_B T = 10^{-3}U_0$, $V = 0.3\omega a$ and $\omega = 2\pi(U_0 N/M)^{1/2}/a$.

$$m\partial^2\mathbf{r}_i/\partial t^2 + \eta\partial(2\mathbf{r}_i - \mathbf{R})/\partial t + \partial[U^{A,B}(\mathbf{r}_i - \mathbf{R}) + U^{A,B}(\mathbf{r}_i)]/\partial\mathbf{r}_i + \sum_{i\neq j}^{N} \partial\Phi(\mathbf{r}_i - \mathbf{r}_j)/\partial\mathbf{r}_j = f_i(t), \qquad i = 1, \ldots, N. \tag{2}$$

Here, we consider a mixed monolayer consisting of two types of molecules A and B, a "base solvent" and an "additive", respectively. Molecules A are numbered from 1 to L and molecules B from L and N. Molecules A and B are chosen in such a way that they tend to occupy different sites on the surfaces of the plates, for instance at the top of a substrate atom and at the center of the substrate lattices. Correspondingly the interactions between each of the plates and molecules A and B are given by different periodic potentials, namely $U^A(\mathbf{r}) = U^A[\cos(2\pi x/a) + \cos(2\pi y/a)]$ and $U^B(\mathbf{r}) = -U^B[\cos(2\pi x/a) + \cos(2\pi y/a)]$, where a is the periodicity of the substrate lattices. The A–B intermolecule interaction is described by a potential Φ which includes a short-range repulsion, $C\exp[-(\mathbf{r}_i - \mathbf{r}_j)^2/c^2]$, and a regularized Coulomb interaction, $q_A q_B/[b^2 + (\mathbf{r}_i - \mathbf{r}_j)^2]^{1/2}$, where for the effective charges we assume $q_B = -q_A = q$, and b is a cutoff parameter. The chosen Coulomb interaction provides an attraction between different types of molecules and a repulsion between identical molecules. The parameter η accounts for the dissipation of the kinetic energy of each particle due to interactions with excitations in the plates. For simplicity we assume that all molecules have the same mass m, dissipation constant η and that $U^A = U^B = U_0$. The effect of the thermal motion of the embedded molecules is given by random forces $f_i(t)$, which are δ-corrected, $\langle f_i(t) f_i(0)\rangle = 2k_B\eta T\delta(t)\delta_{ij}$. T is the temperature and k_B is the Boltzmann constant. The two plates do not interact directly. It should be noted that the particular form of the interactions chosen here serves only as an example to demonstrate the suggested mechanism for tuning friction. However, our conclusions are mostly independent of the particular form of the potentials.

3. Effect of additive concentration

Most studies of frictional forces, using SFA, have focused on the time series of the spring force that represents the lateral response to an external driving force. Before analyzing the model in equations (1) and (2) and describing how to tune friction, we present in figure 2 an example of the dependence of the time-averaged spring force on the concentration ξ of the additive molecules B, where $\xi = (N - L)/N$. The total number of embedded molecules is kept constant. The calculations have been done for three values of driving velocities which correspond to periodic and chaotic stick–slip behaviors which occur at low driving velocities [1–14], and to steady sliding typical of higher velocities. Figure 2 demonstrates a decrease in friction with an increase in the concentration of the additive. A more than fourfold reduction of friction is observed when the concentration of the additive changes from 0 to 0.5. We observe a decrease in friction for all regimes of motion, with the strongest effect at low driving velocities, where

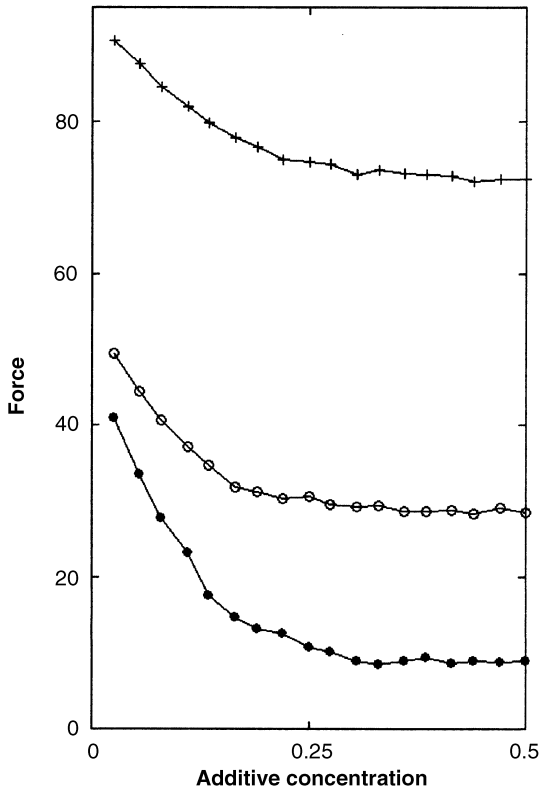

Figure 2. Dependence of average spring force on the concentration of additives for driving velocities $V/\omega a = 0.04$, 0.3 and 0.7 corresponding to stick–slip (•), intermittent type (○) and sliding (+) motions. The force, time and distances are presented in units of $2\pi U_0/a$, $1/\omega = (a/2\pi)(M/U_0N)^{1/2}$ and a. Parameter values are as in figure 1.

the stick–slip motion occurs. Under our assumptions the spring force versus the concentration of the additive molecules is symmetric with respect to $\xi = 0.5$ with a minimum at equal concentrations of the molecules A and B. If we choose molecules with different masses, dissipation constants and/or interaction parameters the corresponding curves will be asymmetric around $\xi = 0.5$.

4. Qualitative discussion in terms of the effective potential

To understand qualitatively the effect of the additives on the system properties it is convenient to look at the effective potential between the A and B particles as a function of the distance between them. This includes the underlying periodic potential, Coulomb interaction and short-range repulsion. Figure 3 shows the evolution of this potential with an increase of the interaction between the molecules. The effective potential exhibits a maximum $U_{\max}$ at short and long A–B distances, separating two minima, which correspond to paired ($U_{\min 1}$) and unpaired ($U_{\min 2}$) configurations of the A and B molecules. The deeper the minimum, the more probable is the corresponding configuration. The probability of transitions between the states is defined by the difference between the maximum of the energy and the relevant minimum. Evolution of the positions of the maximum and minimum (up to their merging) with the increase in the attraction is shown in figure 3 by points and stars, respectively. There are three critical values of the attraction parameter q: q_1, q_2 and q_3. When $q < q_1$ pairs

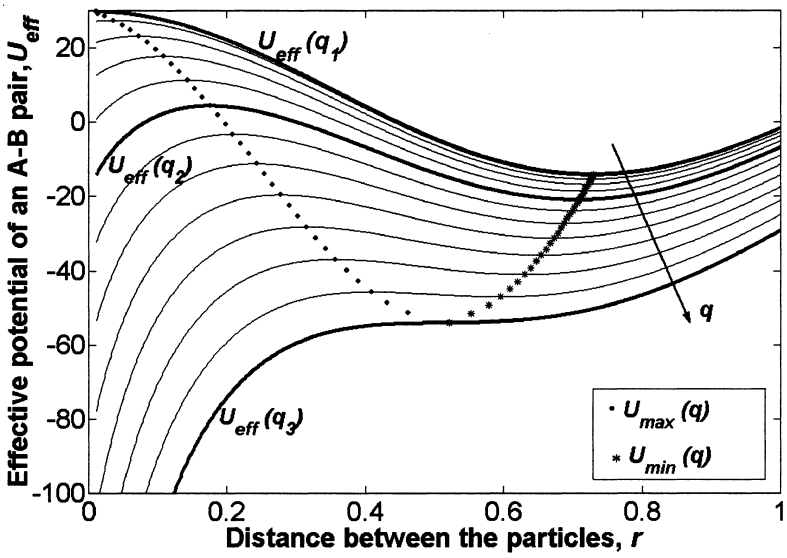

Figure 3. Effective potential U_{eff} of an A–B pair versus the distance r between A and B molecules at different attraction strengths q (q increases from the top down). The maximum of the potential (•) separates two minima (*), corresponding to paired (at $r = 0$) and unpaired A–B states. Effective potentials $U_{\text{eff}}(q_1)$, $U_{\text{eff}}(q_2)$, $U_{\text{eff}}(q_3)$ at critical values of the attraction parameter are marked by bold lines. Parameter values are as in figure 1.

are never formed. The binodal energy corresponds to $q = q_2$, at which the paired and unpaired configurations are equally probable. For $q > q_3$, the minimum $U_{\min 2}$ disappears and only the paired A and B particles are expected to be found.

5. Shear-induced phase transitions and frictional response

In order to clarify the proposed mechanism for tuning friction by adding an additive, we have performed a detailed study of the geometrical structure of the mixed embedded molecular layer under shear, and have established the relationship between geometry and frictional response. Here we present results obtained for the additive concentration $\xi = 0.5$ which corresponds to an equal number of A and B molecules. Figure 4 shows the time series of the spring force and of the ensemble-averaged distance between the molecules. Both are calculated for weak, intermediate and strong attractions between the solvent and additive molecules. In our model, the strength of the attraction is determined by the "effective charge" of the molecules, q. All the curves in figure 4 have been obtained for the same driving velocity which corresponds to stick–slip motion for the base solvent A. In addition, figure 1 shows snapshots of the embedded system observed during stick and sliding states of motion for the intermediate strength of attraction. The instants corresponding to the snapshots are marked on the time series of the force by arrows in figure 4(b). The snapshots are complemented by the two-dimensional (2D) Fourier transforms of the instantaneous correlation function for the sheared monolayer, which are also shown in figure 1.

Our results clearly demonstrates that for weak and intermediate strengths of the A–B attraction the monolayer in the stick state has a *tetragonal* symmetry, for which the distances between neighboring A–A and A–B molecules equal a and $a/\sqrt{2}$, respectively. For the weak attraction the monolayer retains also the tetragonal symmetry in the sliding state where the monolayer molecules move mostly while remaining in the corresponding minima of the molecular-plate potentials. This is reflected in the time series of the averaged distance between A–B neighbors, which only slightly fluctuates around the value of $a/\sqrt{2}$ (figure 4(a)). The same is true for the monolayer containing only one kind of molecule.

In contrast, for the intermediate A–B attraction a new *hexagonal* symmetry arises during sliding. Here the two types of molecules group into A–B pairs and form a lattice with well-defined hexagonal symmetry, essentially ignoring the symmetry of the underlying potential (see figure 1). The effect of pair formation is seen in figure 4(b), which shows a significant decrease of the A–B distances during sliding compared to the value $a/\sqrt{2}$ that is typical of the tetragonal lattice. Sliding and stick states can be easily distinguished according to the time series of the spring force shown in figure 4. Our calculations also demonstrate that, being in the sliding state, the molecules are, on average, equally distant from the minima of the plate potentials $U^{\mathrm{A}}(\mathbf{R})$ and $U^{\mathrm{B}}(\mathbf{R})$ and move within the channels between them. Thus, due to

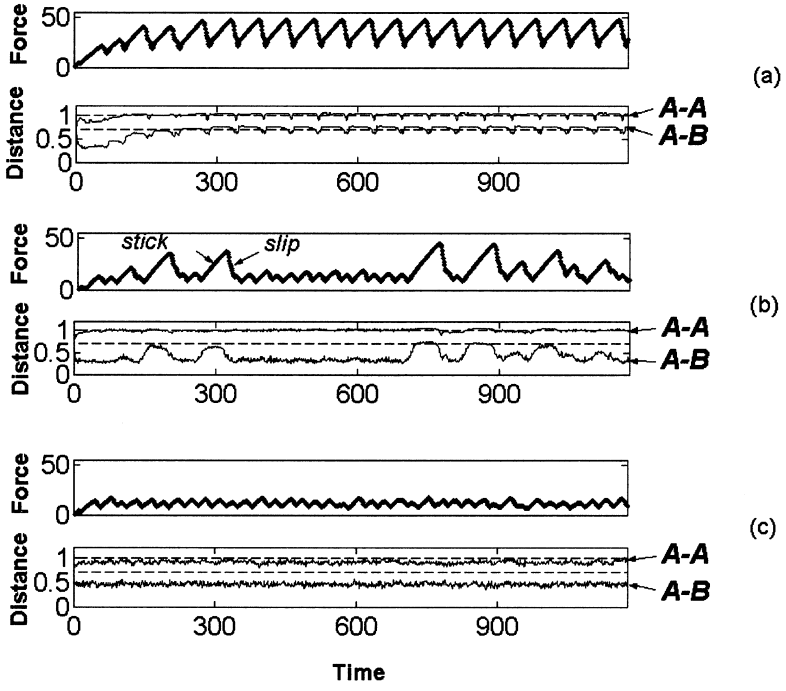

Figure 4. Time dependence of the spring force for different attraction values: (a) weak $q/(U_0 a)^{1/2} = 0.5$, (b) intermediate $q/(U_0 a)^{1/2} = 0.9$ and (c) strong $q/(U_0 a)^{1/2} = 1.4$. The lower panel of each shows the corresponding time dependence of the distances between neighboring A and B molecules. Parameter values: $V = 0.07\omega a$, $\eta = 2.6M\omega/N$, $N = 50$; other parameters as in figure 1.

the intermolecular attraction between the base and additive, the molecules "pull" each other out of the minima of the corresponding potentials U^{A} and U^{B}, effectively decreasing the potential barriers to sliding. This leads to a significant reduction of friction force in the sliding state, and to an increase of time intervals that the system spends in motion.

As noted above, for intermediate strengths of attraction the embedded monolayer has mostly tetragonal symmetry in the stick state. However, A–B attraction causes the formation of defects: pairs, pair chains and domains of a foreign phase within the tetragonal lattice. The presence of defects leads to a decrease in the external force needed to initiate motion (depinning force) as compared with the cases of weak attraction and of a monolayer containing only one kind of molecule. In this way the A–B attraction reduces the time-averaged depinning force (static friction) and transforms the almost periodic stick–slip motion into an erratic one (compare figures 4(a) and 4(b)). However, figure 4(b) shows that from time to time an almost ideal tetragonal structure with A–B neighboring distances close to $A/\sqrt{2}$ builds up, accompanied by an enhancement of the instant depinning force. This occurs as a result of the effective stirring of the system, which can take place during long intervals of sliding motion. Such a motion induces annealing, which removes defects that always arise under preparation of the system, off the tetragonal lattice.

For strong A–B attraction we find that the embedded molecules form at all times a nonideal hexagonal lattice, which includes pair chains and dislocations. Many sites are found to have a local symmetry of the fifth–seventh order. Figure 4(c) shows that at all times the molecules coalesce into A–B pairs drastically reducing the frictional force. In this case the system executes sliding motion even in the range of low driving velocities, where a stick–slip motion has been observed for weak and intermediate strengths of attraction.

6. Analysis of the geometrical structure of the sheared layer

6.1. Density of states

The effect of the rearrangement in the mixed system under shear is clearly reflected in the time-averaged density of states, which provides the probability of finding a pair of molecules with a given distance between them. One can study separately the distances between identical A–A and different A–B molecules. It is also useful to distinguish between contributions of the stick and sliding intervals to the density of states [19]. As a result, there are four separate contributions to the density of states shown in figure 5. (Here, the states with a top plate velocity less than $0.25V$ were considered as the stick states and all other states as the sliding ones. The value $0.25V$ lies approximately half way between the typical maxima of the density corresponding to the sliding and the stick states.) All the contributions to the density of states are normalized to the total number of states. Thus, the contributions of stick and sliding states to the total distribution are proportional to the duration of the corresponding state.

Figure 5 shows that at weak attraction the most probable distances between A–B molecules lie around $a/\sqrt{2}$, while those between A–A molecules are con-

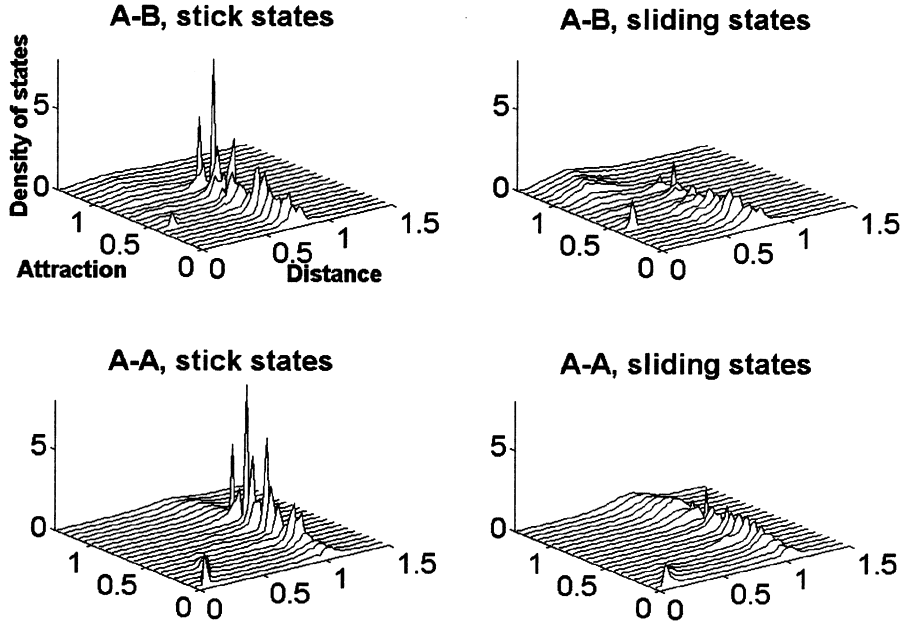

Figure 5. Contributions to the density of states with given distances between the A–B and A–A molecules. Parameter values: $N = 72$, $\eta = 2.6M\omega/N$; other parameters as in figure 1.

centrated around a. These values are natural for the tegragonal lattice. It should also be noted that a weak interaction cannot separate the A–A pairs, which are virtually frozen from an initial random configuration of the molecules. Such pairs survive for a long time and give rise to the additional maxima, which are seen in the A–A density of states in figure 5 for weak interactions.

When the interaction exceeds some critical value $q = q_1$, A–B pairing becomes possible. It causes an appropriate maximum in the density of states above $q = q_1$. At the same time, the increase of the interaction improves the effective annealing of the frozen defects. The annealing competes with the A–B pairing at the intermediate strength of interactions and even leads to the formation of the ideal tetragonal lattice at some values of the interaction. This tetragonal configuration corresponds to sharp maxima in the density of states at the distances a and $a/\sqrt{2}$, which are clearly seen in the A–A and A–B subplots for the stick states in figure 5. It is also slightly reflected by the small narrow maxima in the subplots corresponding to the sliding states. Physically it means that due to the effective "annealing" during long periods of sliding, the molecules manage to occupy the minima of the substrate potential almost ideally.

For strong attraction, the contribution of the sliding states dominates over that of the stick states, and the embedded system spends most of the time in the hexagonal configuration with the A–B molecules grouped into pairs. This corresponds to a density that is concentrated around the distance typical for the hexagonal structure.

As the attraction increases further, all the contributions to the density distribution become smeared out and tend towards a universal density distribution

$$P = (a^2/2\pi)r \exp(-\pi r^2/a^2) \qquad (3)$$

characteristic of a system of randomly distributed particles (see appendix A). This randomization is caused by the many-body nature of the system, which results in a transformation of the energy of interactions into a thermal energy. This process is more effective for stronger interactions between the particles and/or for higher driving velocities. As a result of such well-known thermalization of the dynamical system [20], the densities of states approach asymptotically the universal one found for the randomly distributed particles.

6.2. Fraction of paired solvent–additive molecules

The calculated density of states allows the fraction of A–B pairs at any value of attraction to be found. Figure 6 shows the fraction of pairs (bold line) as well as the contributions to it from the intervals of stick and sliding (thin lines) which have been obtained by integrating the density of states.

Besides the obvious increase of the fraction of A–B pairs with the interaction, one can see fine structure in the curves, which corresponds to the mixed state including both paired and unpaired A–B configurations. In particular, there is a well-pronounced maximum at intermediate interactions, $q \approx 1$. This maximum corresponds to the A–B pairs that survive from the initial random configuration.

The observed behavior of the fraction of A–B pairs can be understood qualitatively, and described analytically, using the effective potential shown in figure 3. The probability that the A–B molecules are paired (or unpaired) is determined by the relationship between the energies of the corresponding minima and the energy of

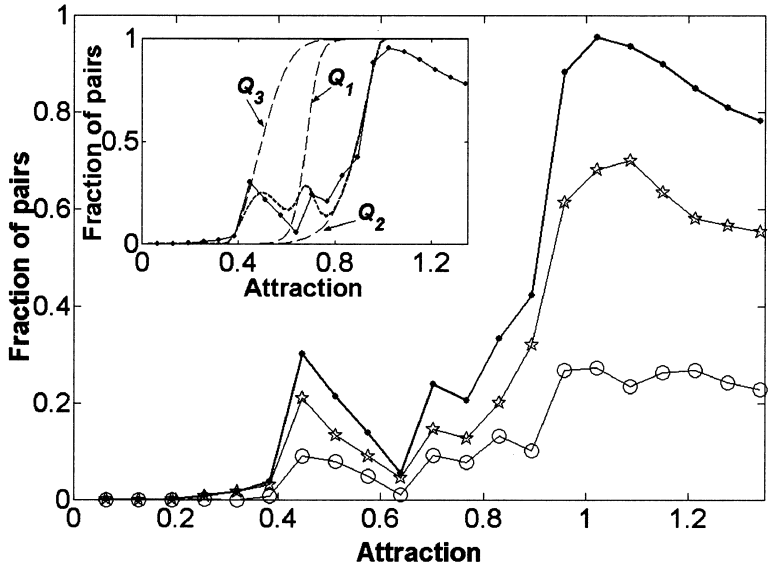

Figure 6. Fraction of pairs among A–B molecules in the stick states (○), in the sliding states (☆) and the total fraction of pairs (bold line) as a function of A–B attraction. The inset shows analytical estimations of the fractions of pairs Q_1, Q_2, Q_3 and of the total fraction of pairs Q (bold dashed line) versus q fitting the numerical result (solid line). Parameter values: $N = 72$, $\eta = 2.6M\omega/N$, $V = 0.04\omega a$; other parameters as in figure 1.

the maximum that separates them. It is convenient to introduce the following three probabilities:

$$Q_1 = 1/\{1 + \exp[-U_{\min 2} - U_{\min 1})/kT]\}, \quad (4)$$

$$Q_2 = \exp[-(U_{\max} - U_{\min 2})/kT], \quad (5)$$

$$Q_3 = 1 - \exp[-(U_{\max} - U_{\min 1})/kT]. \quad (6)$$

Here, Q_1 is the probability for A–B molecules to become paired at equilibrium in the absence of the external drive. The probabilities Q_2 and Q_3 account for a nonequilibrium nature of the system under shear. Q_2 is the probability for A–B molecules to become paired from the unpaired configuration and Q_3 is the probability for A–B molecules to stay paired if they are initially paired. The dependencies of Q_1, Q_2 and Q_3 on the strength of the interaction are shown in the insert to figure 6.

It should be noted that the number of paired (unpaired) molecules at the beginning of each stick interval is determined by how the ideal tetragonal configuration is formed immediately after sliding. This depends on the effectiveness of annealing the defects during sliding, which depends on the duration of the sliding states. The latter, as we saw, is proportional to the fraction of paired molecules. This fraction is determined by Q_3 for weak attraction and by Q_1 for stronger attractions. Thus, the final estimate Q for the fraction of pairs can be written as

$$Q = Q_2 Q_1 + Q_1(1 - Q_1) + Q_3(1 - Q_3). \quad (7)$$

Figure 6 shows that this analytical expression, together with equations (4)–(6), fits the numerical data rather well.

The fraction of pairs saturates, $Q \approx 1$, around the second critical interaction parameter $q = q_2$. However, at stronger interactions it falls again. This is caused by the effect of thermalization of the system at strong interactions, which is discussed above. In this region the dynamics of the system looks similar to that determined by a random noise. All the distributions become smeared, and the asymptotic value of the fraction of pairs tends to 0.5.

The dependence of the fraction A–B pairs on the intensity of random noise is shown in figure 7. As has already been discussed, this curve cannot be described by the equilibrium fraction of pairs, Q_1. It also includes corrections due to the transitions between paired and unpaired states. For low-noise values the calculated curve deviates from Q_1 due to the contribution of shear-induced transitions from unpaired to paired states. For high-noise values the transitions from paired to unpaired states contribute essentially to the calculated fraction of pairs. As expected, in this case the curve approaches the asymptotic value 0.5.

6.3. Dynamical phase diagram

The accumulated fraction Q of A–B at different values of the attraction and driving velocity allows a phase diagram of the embedded system under shear to be built (figure 8). It shows two asymptotic ordered phases: the tetragonal phase, which exists in the region of weak attraction and low driving velocity V, and the hexagonal phase for high attraction parameter q. These phases are separated by a mixed phase where the tetra-

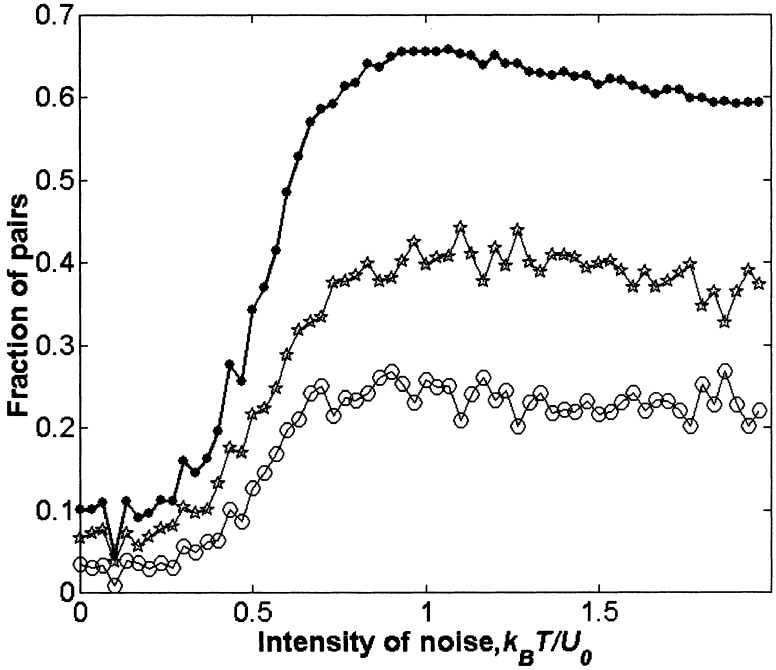

Figure 7. Fraction of pairs among A–B molecules in the stick states (○), in the sliding states (☆) and the total fraction of pairs (bold line) as a function of the intensity of the external noise. Parameter values: $N = 72$, $\eta = M\omega/N$, $V = 0.04\omega a$; other parameters as in figure 1.

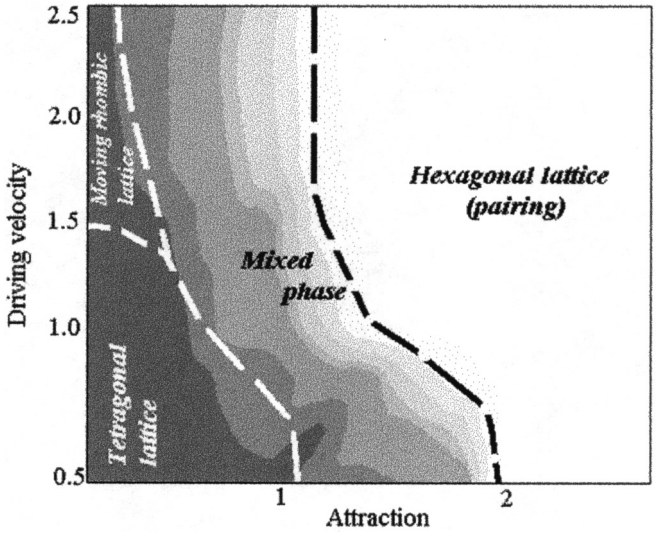

Figure 8. Phase diagram of the embedded monolayer under shear, showing the fraction of A–B pairs (the decrease in the fraction of pairs is shown by variation of the color from dark to light) at different values of attraction and driving velocity. Parameter values: $N = 72$; other parameters as in figure 1.

gonal and hexagonal domains coexist. In the mixed phase the transitions between hexagonal and tetragonal states take place during stick–slip events.

An additional phase can be distinguished, which is located at high driving velocities and weak attractions. It can be defined as the sliding rhombic phase. In this phase the lattice of the molecules, as a whole, is pulled out of the potential minima created by the plates, so that its tetragonal symmetry is only slightly deformed during the transition to sliding.

Shear-induced transitions between tetragonal and hexagonal phases observed here resemble the Kosterlitz–Thouless transitions in 2D systems with Coulomb interactions, where pairing–unpairing of oppositely charged particles occurs under a change of the balance between interaction and temperature [21]. In our case the pairing–unpairing is mainly controlled by the balance between periodic potentials and interaction strength. Here an external force shifts the particles from the potential minima so that the plate velocity rather than temperature plays the role of the characteristic parameter that triggers the transition. The driven system resides alternately in both Kosterlitz–Thouless phases, and their contributions to the average are dictated by the duration of the stay in each phase. Coexistence of the tetragonal and hexagonal phases has been also observed here at every instant in the form of domains of one phase inside another. Because of competition between the interactions, as well as strong fluctuations typical of 2D systems, neither ideal tetragonal nor ideal hexagonal lattices have been observed under shear.

7. Tuning friction by intermolecule interaction

In order to characterize quantitatively the effect of A–B attraction on the frictional force, we present in figure 9 the time-averaged frictional forces as a function of the attraction parameter in three typical regimes of motion: stick–slip, intermittent motion and sliding. A significant reduction in friction with an increase in attraction has been found in all regimes. However, the strongest effect (a 12-fold reduction of the force for particular chosen parameters) has been observed for the smallest driving velocity, which corresponds to a periodic stick–slip motion in a system with one kind of molecule.

This observation can be understood by taking into account that there are two contributions to the frictional force: (i) the potential terms U^{A} and U^{B} in equation (1), and (ii) the viscous term given by $\sum_i^N \eta\partial(\mathbf{R} - \mathbf{r}_i)/\partial t$. The potentials U^{A} and U^{B} dominate in the stick–slip regime (the tetragonal structure), and contribute an estimated averaged force of $\pi U_0 N/b$ [5]. The attraction between A and B molecules reduces the effective potential barriers, so the potential contribution to friction decreases significantly with the attraction. The viscous contribution is constrained in the range between ηVN and $\eta VN/2$ [5]. Thus, at low driving velocities the reduction of friction can be as large as $(\pi U_0/b + \eta V)/(\eta V/2)$.

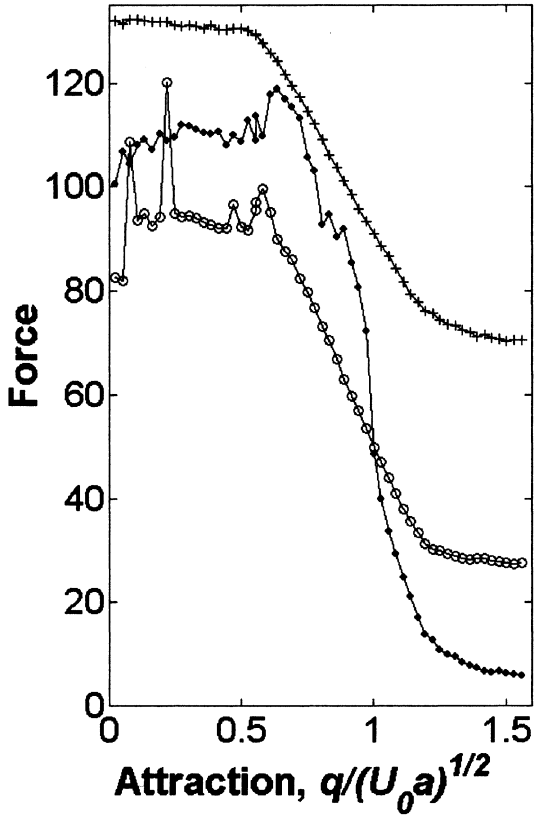

Figure 9. Time-averaged spring force as a function of attraction for driving velocities $V/\omega a = 0.04$, 0.3 and 0.7 corresponding to stick–slip (•), intermittent type (○) and sliding (+) motions. Parameter values are as in figure 1.

The viscous term dominates the sliding regime. The A–B attraction also influences the viscous contribution by suppressing the velocity fluctuations of the embedded molecules. However, due to the above-mentioned constraints on the value of the viscous term [5], this effect is less pronounced than the effect of the attraction on the potential contribution. As a result, for high driving velocities, where the potential contribution is less important, the reduction does not exceed a factor of 2. The effect of velocity on the reduction of friction is clearly seen in figures 2 and 9, where the dependence of the friction on the concentration of additive B and on the strength of attraction is shown. The saturation in the reduction of friction for a strong attraction, which is evident in figure 9, is also explained by the constraints on the viscous term, which is bounded from below by the value $\eta VN/2$.

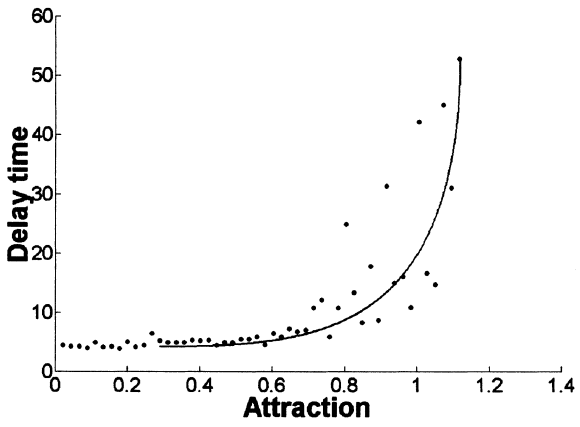

Figure 10. Delay time τ^* as a function of A–B attraction, obtained from numerical stop–start experiments (•) and by the method of least squares (line). Parameter values: $N = 50$, $M/m = 70N$, $\eta = 10M\omega/N$, $V = 0.1$; other parameters as in figure 1.

8. Stop–start experiments

Additional information on the shear-induced phase transitions can be extracted from stop–start experiments. It has been demonstrated [22] that if during sliding the external drive is stopped for a certain time τ smaller than some upper limit τ^* and then reinitiated with the same velocity, the additional static force $\Delta F_s = F_s - F_k$ (where F_s and F_k denote the static and kinetic friction force, respectively) to be overcome might vanish, thereby giving rise to an interesting memory effect.

These stop–start experiments allow one to estimate a relaxation time in the embedded system. Here, in order to find the relaxation time, we followed the averaged velocity of the embedded molecules during stop–start experiments, which is well correlated with the experimentally observed behavior of the spring force. We found that for $\tau > \tau^*$, the particles slow down and their velocity decreases below a threshold value, corresponding to the stick state before resuming the drive. For $\tau < \tau^*$ the slowing of the molecules is not significant and they are "picked up" by the reinitiated external drive while running. Based on the correlation between the macroscopic response of the spring force and the microscopic response of the particle behavior, we have used the latter to define the delay time in the numerical experiments. The delay time versus A–B attraction is plotted in figure 10. This plot indicates the substantial increase in the delay time with the A–B attraction. There are two reasons for this phenomenon: (i) the intermolecule attraction reduces the effective potential barrier experienced by the molecules, which promotes sliding and (ii) in the mixed system the symmetries of the layer in the sliding and stick states are different, which slows down the transition between them and prolongs the delay time.

An analytical estimate of the delay time observed in our numerical stop–start experiment can be found from the following consideration. Pairing that occurs in the sliding regime leads to an increase of the energy of the system compared to that in the tetragonal configuration where molecules are located in the minima of the combined potential. This excess energy should be dissipated during the transition from the sliding to the stick state. A characteristic time for this relaxation can be approximated by the equation

$$\tau \propto \ln(1 + \Delta U(x)/U_0), \tag{7}$$

where $x = (1 - \sqrt{2}r)/2$ is a shear-induced displacement of the molecule from the potential minimum due to pairing, which can be estimated from the balance of forces acting on the molecule:

$$\frac{q^2}{r^2} - \frac{4\sqrt{2}\pi}{a} U_0 \sin\left[\frac{\pi}{a}(1 - r\sqrt{2})\right] - \frac{2C}{c} r \exp(-r^2/c) = 0, \tag{8}$$

and $\Delta U \approx 4U_0 N \cos(\pi x/a\sqrt{2})$ is the difference between the energies of the system in the paired and unpaired configurations. A comparison of the numerical data with the calculations according equations (7) and (8) is shown in figure 10. A good agreement between numerical and theoretical results confirms the adequacy of the suggested mechanism of memory effect.

9. Control of the regimes of motion

Mixing the embedded layer with additives not only reduces friction and increases the delay time, but it also makes it possible to control the regimes of motion. That is, tuning the concentration of additives or/and the attraction between the additive and the base solvent allows stick–slip motion to be eliminated and sliding to

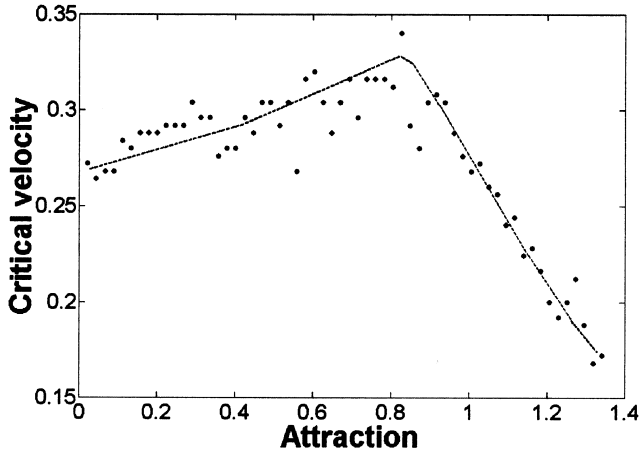

Figure 11. Critical velocity of the transition from stick–slip motion to steady sliding of the top plate as a function of the A–B attraction q. Parameters values: $N = 50$; other parameters as in figure 1.

be achieved at low driving velocities (see figures 4(a) and 4(c)). As an illustration, figure 11 shows the critical velocity corresponding to the transition from stick–slip motion to sliding as a function of the attraction. This curve has two characteristic features: a shallow increase of critical velolcity at weak–intermediate interactions and a steep decrease of critical velocity for the stronger attraction.

The first effect can be understood by taking into account the fact that in the present model the A–A repulsion increases along with the increase in A–B attraction. The repulsion prevents the formation of defects (A–A pairs) and favors an ideal tetragonal arrangement in which the molecules have to overcome the highest potential barriers during motion. As a result, the sliding regime begins at a higher driving velocity. The second effect, observed at strong attraction, is explained by pairing of A–B molecules, which leads to a decrease of the effective potential barriers and reduces the critical velocity. Such a possibility of controlling the regimes of motion can be of great technological importance for micromechanical devices, where the early stages of motion and the stopping processes, which exhibit stick–slip, pose a real problem.

10. Conclusions

A new approach has been suggested for controlling frictional forces and obtaining desirable phases of motion. A model has been introduced, which simulates the SFA arrangement with an embedded monolayer consisting of two kinds of molecules—base A and additive B. We have found that the symmetry of the embedded mixed layer changes during stick–slip transitions due to shear-induced phase transitions. A phase diagram of the embedded system under shear has been built in driving velocity–attraction coordinates, where tetragonal and hexagonal asymptotic ordered phases, separated by a mixed one, as well as an additional rhombic phase have been distinguished. Due to the phase transition, tuning of the frictional forces by adding the additives is achieved. The effect of the rearrangement in the layer under shear is clearly seen in the density of states of the embedded system. We calculated the fraction A–B pairs as a function of the strength of attraction using the density distribution. It is shown that A–B pairing effectively reduces the potential barrier that needs to be overcome for initiating sliding. The effect of A–B attraction on the frictional force has been characterized quantitatively by studying the time-averaged frictional forces in three typical regimes of motion as a function of the attraction parameter. The maximum possible value of the reduction of friction has been estimated by separating the potential and viscous contributions to the frictional force. We have shown that mixing the embedded layer with additives not only reduces friction and increases the delay time, but it also makes it possible to control the regimes of motion. In particular, increasing the A–B attraction strength allows the stick–slip regime to be eliminated and steady sliding to be reached at low driving velocity. In addition, shear-induced phase transitions result in a significant increase of relaxation time of the embedded system (memory effect), which can be measured in stop–start experiments.

Acknowledgement

Financial support for this work by grants from the Israel Science Foundation, BSF, TMR-SISITOMAS and DIP is gratefully acknowledged.

Appendix A

Here we calculate the probability of finding a nearest neighbor at a distance r in the system of randomly distributed particles. This probability can be presented as a product of two factors: the probability P_r of finding a particle in the interval $[r, r + \mathrm{d}r]$

$$P_r \sim r\mathrm{d}r, \tag{A1}$$

and the probability P_S that there are no particles inside a circle with radius r

$$P_S \sim (1 - \pi r^2/S)^N, \tag{A2}$$

where S is the area of the system of N particles. So, when the number of particles tends to infinity the required

probability is $P \sim \lim_{N\to\infty}[P_r P_S(N)]$. Finally, for the density distribution one has

$$P = r\,\exp(-\pi r^2/a^2)/\int r\,\exp(-\pi r^2/a^2)\mathrm{d}r$$
$$= (a^2/2\pi)r\,\exp(-\pi r^2/a^2). \quad \text{(A3)}$$

References

[1] B. Bhushan, J.N. Israelachvili and U. Landman, *Nature* **374** (1995) 607.
[2] J. Klein and E. Kumacheva, *Science* **269** (1995) 816.
[3] S. Granick, *Phys. Today* **52** (1999) 26.
[4] G. Hanhner and N.D. Spencer, *Phys. Today* **51** (1998) 22.
[5] M.G. Rozman, M. Urbakh, J. Klafter and F.J. Elmer, *J. Phys. Chem.* **102** (1998) 7924.
[6] G. He, M.H. Muser and M.O. Robbins, *Science* **284** (1999) 1650.
[7] B.N.J. Persson, *Sliding Friction. Physical Principles and Applications* (Springer, Berlin, 2000).
[8] F. Family, H.G.E. Hentschel and Y. Braiman, *J. Phys. Chem.* B**104** (2000) 3984.
[9] H.-W. Hu, G.A. Carson and S. Granick, *Phys. Rev. Lett.* **66** (1991) 2758.
[10] P.A. Thompson, M.O. Robbins and G.S. Greast, *Israel J. Chem.* **35** (1995) 93.
[11] M.G. Rozman, M. Urbakh and J. Klafter, *Phys. Rev. Lett.* **77** (1996) 683.
[12] E. Kumacheva and J. Klein, *J. Chem. Phys.* **108** (1998) 7010.
[13] V. Zaloj, M. Urbakh and J. Klafter, *Phys. Rev. Lett.* **82** (1999) 4823.
[14] C. Drummond and J. Israelachvili, *Phys. Rev. E* **63** (2001) 041506.
[15] A.G. Papay, *Lubr. Eng.* **47** (1991) 271.
[16] T. Kugimiya *et al.*, *SAE paper* 952348 (1995).
[17] M. Ruths, H. Ohtani, M. L. Greenfield and S. Granick, *Tribol. Lett.* **6** (1999) 207.
[18] M.L. Greenfield and H. Ohtani, *Tribol. Lett.* **7** (1999) 137.
[19] A.E. Filippov, J. Klafter and M. Urbakh, *Phys. Rev. Lett.* (in press).
[20] R.Z. Sagdeev, D.A. Usikov and G.M. Zaslavsky, *Nonlinear Physics: From the Pendulum to Turbulence and Chaos* (Harwood Academic, 1992).
[21] J.M. Kosterlitz and D.J. Thouless, *J. Phys. C: Solid State Phys.* **6** (1973) 1181.
[22] H. Yoshizawa and J. Israelachvili, *J. Phys. Chem.* **97** (1993) 11300.